Flight testing of the VT-03-s Shadow Multi-Tilt-Rotor Configuration with a Maneuver Control System Enabling Simplified Vehicle Operations and Tactical Maneuvering

Imon Chakraborty Associate Professor
Bikash Kunwar Graduate Student
Stefanus Harris Putra Graduate Student
Rajan Bhandari Graduate Student
Cole McCormick Graduate Student
Vehicle Systems, Dynamics, and Design Laboratory (VSDDL)
Auburn University
Auburn, AL, USA

ABSTRACT

This work describes the flight control system architecture of the VSDDL VT-03-s Shadow, a cost-effective subscale aircraft used as a testbed for novel flight control schemes. The highlight is the Maneuver Control System comprising the Trajectory Control System, which facilitates Simplified Vehicle Operations, and the Tactical Maneuvering System, which permits more aggressive maneuvering. The control laws permit the selection of both vertical takeoff and landing and conventional takeoff and landing modes of operation. Flight test results shown include transitions between vertical and forward flight modes performed using both Trajectory Control System and Tactical Maneuvering System, limited aerobatic maneuvering performed using the Tactical Maneuvering System, and demonstration of some of the automatic flight functions and capabilities.

INTRODUCTION

Simplified Vehicle Operations (SVO) (Ref. 1) is an operational paradigm that aims to reduce pilot workload through the integrated design of flight control laws, inceptors, and cockpit displays. Prior work by the Vehicle Systems, Dynamics, and Design Laboratory (VSDDL) demonstrated SVO-centric flight control system (FCS) architectures for several vertical takeoff and landing (VTOL) configurations, including lift-plus-cruise (Refs. 2–4) and tilt-wing (Refs. 5–8) designs through both simulation and subscale flight-testing.

These SVO-centric FCS architectures featured the Trajectory Control System (TCS)[1], a middle-loop controller coordinating propulsor thrust, thrust inclination (when applicable), and aircraft pitch attitude. Prior work successfully demonstrated TCS for transitioning lift-plus-cruise (Refs. 7, 9), tilt-wing (Refs. 7, 8), and vectored-thrust (Refs. 7, 10, 11) configurations, in each case enabling a minimally trained operator to control a transitioning VTOL aircraft.

While TCS is a substantial enabler for SVO, the necessary envelope protection through rate and attitude limits makes it unsuitable for aggressive or tactical maneuvering. The Tactical Maneuvering System (TMS) was developed to address this limitation and allow the full maneuvering potential of the aircraft to be exploited by a skilled pilot. Prior work by the authors (Ref. 12) demonstrated (through simulation) an early implementation of TMS for a tilt-wing configuration. TCS and TMS control laws are harmonized within the Maneuver Control System (MCS), a middle-loop controller that allows seamless in-flight switching between the two control schemes. This versatile control solution, which has been flight-tested, allows mission-driven selection of either SVO or tactical control modes on the same vehicle within the same FCS architecture.

Further, the demonstrated FCS architecture permits conventional takeoff and landing (CTOL) in addition to VTOL. Even for VTOL aircraft, having CTOL capability can be an advantage as CTOL operations (when possible) allow energy savings by avoiding the high power demands of vertical flight. They are also a valuable contingency option in degraded (post-failure) scenarios where decelerating to vertical flight for landing is either impossible or inadvisable due to high risk.

Salient features of the FCS architecture and flight-test results are presented for the VSDDL VT-03-s Shadow vectored thrust configuration. The flight-test campaign involved substantial use of a dual-purpose ground control station (GCS) that was used in simulation mode in the laboratory for control law development and testing and then in flight-test mode in the field.

VT-03-S SHADOW SUBSCALE AIRCRAFT

The VT-03-s Shadow (VT: vectored thrust, -s: subscale), shown in Fig. 1, is a vectored thrust VTOL/CTOL-capable subscale aircraft based on the NASA Langley Research Center RAVEN-SWFT configuration (Ref. 13). It features a high-wing, a conventional tail, and a fixed tricycle landing gear with a castering nosewheel. The propulsion system consists of six propulsors: four individually actuated

[1]PCT Patent Application No.: PCT/US2025/040100

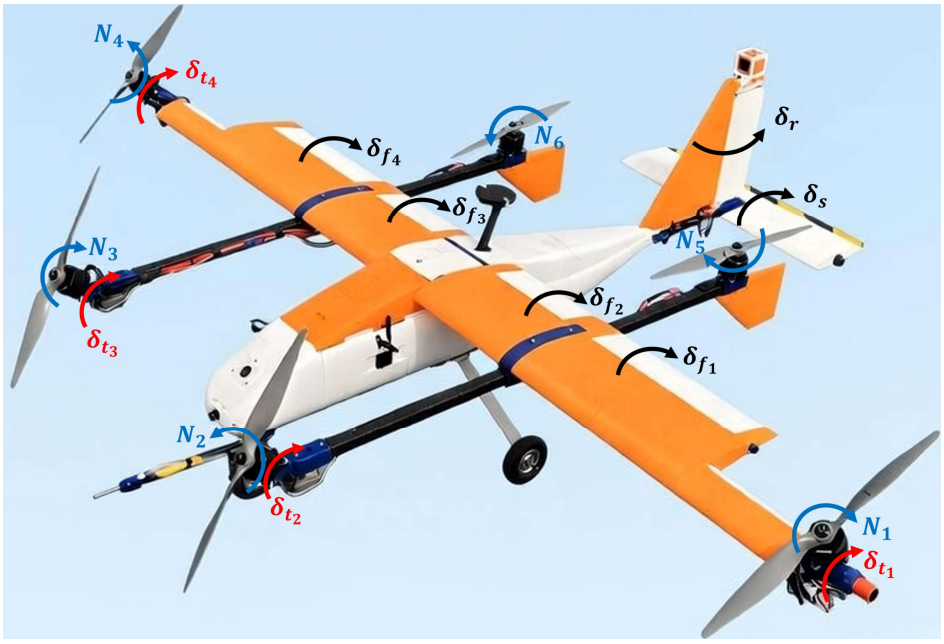

Figure 1. VT-03-s Shadow propulsor and control surface definitions

tilting main propulsors (two at the wingtips, two on the front ends of the wing-mounted booms) and two fixed lift propulsors (at the aft ends of the booms). Each propulsor comprises a motor directly driving a fixed-pitch propeller. Key aircraft characteristics are shown in Table 1. The control effectors are listed in Table 2 and shown in Fig. 1.

In hovering flight, the main propulsors are oriented vertically. Differential thrust (RPM) between propulsors (N_1, N_2, N_5) and (N_3, N_4, N_6) is used for roll control. Differential thrust (RPM) between propulsors (N_2, N_3) and (N_5, N_6) is used for pitch control. Yaw is controlled by differential tilt of the wingtip nacelles (δ_{t_1}) and (δ_{t_4}), to which the outboard wing panels are keyed.

As the aircraft accelerates, the main propulsors progressively tilt forward, the wing generates progressive more aerodynamic lift, and the lift propulsors gradually power down. In forward flight and CTOL operations, the main propulsors assume a horizontal orientation and the lift propulsors are inactive. Inboard and midboard flaperons on the wing are used for roll control, an all-moving stabilator is used for pitch control, and a rudder on the vertical stabilizer is used for yaw control. When operating on the ground in CTOL mode, differential thrust from the forward-facing main propulsors aids in ground steering.

Table 1. VT-03-s Shadow - key characteristics

Propulsion	
Motors (×6)	T-MOTOR AM480 650KV
Main Propeller (×4)	APC 15×10 E/EP fixed-pitch
Lift Propeller (×2)	APC 15×4 E/EP fixed-pitch
Main Battery	Hoovoo 10000 mAh 6S LiPo
Avionics Battery	HRB 3000 mAh 4S LiPo
Avionics & Sensors	
Flight Controller	CubePilot Cube Orange
GPS	Here3+ GPS
Airspeed Sensor	MATEKSYS ASPD-4525
LiDAR	TFmini-S
Telemetry	RFD 900X-US
FPV	Walksnail Avatar GT digital
Geometry	
Wingspan	1.7 m / 5.6 ft
Length	1.32 m / 4.32 ft (excluding pitot)
Length	1.60 m / 5.24 ft (including pitot)
Mass Properties	
Gross Weight	7.89 kg / 17.39 lb
Body-fixed axes	forward-right-down
Origin	Nacelle 1,4 pivot axis on CL
x_{cg}, y_{cg}, z_{cg}	{0,0,6.20} cm / {0,0,2.44} in
Inertias I_{xx}, I_{yy}, I_{zz}	1.35, 0.82, 1.72 kg·m^2

Table 2. List of VT-03-s Shadow control effectors

#	Symbol	Description	Unit
1	δ_{f_1}	Left midboard flaperon	deg
2	δ_{f_2}	Left inboard flaperon	deg
3	δ_{f_3}	Right inboard flaperon	deg
4	δ_{f_4}	Right midboard flaperon	deg
5	δ_s	Stabilator	deg
6	δ_r	Rudder	deg
7	δ_{t_1}	Propulsor #1 nacelle angle	deg
8	δ_{t_2}	Propulsor #2 nacelle angle	deg
9	δ_{t_3}	Propulsor #3 nacelle angle	deg
10	δ_{t_4}	Propulsor #4 nacelle angle	deg
11–14	N_1–N_4	Main propulsor RPMs	RPM
15–16	N_5, N_6	Lift propulsor RPMs	RPM

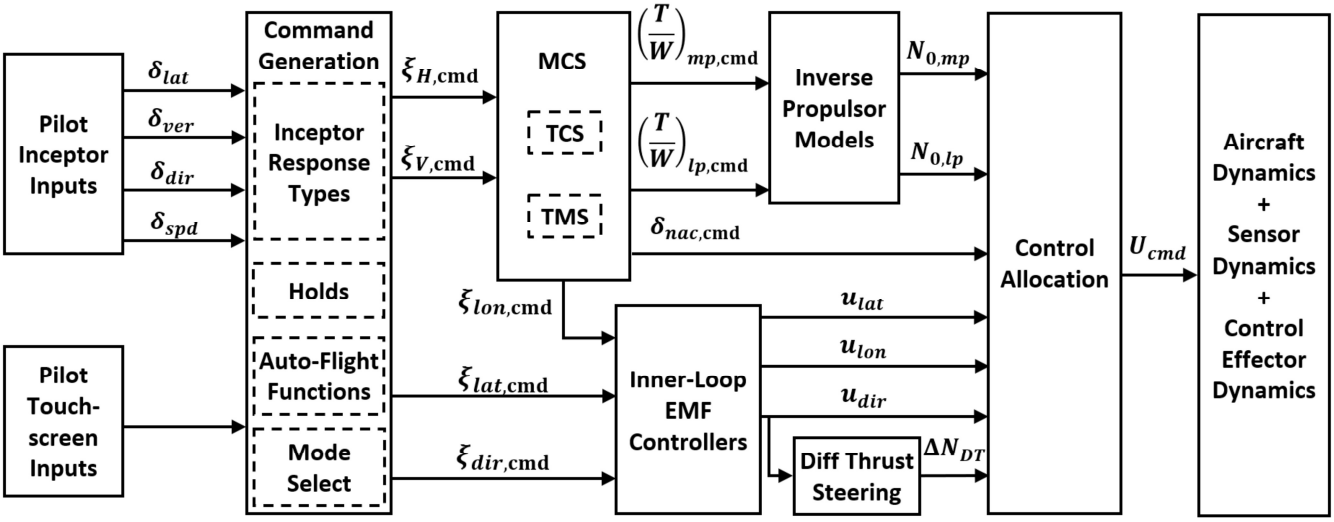

Figure 2. Flight control system architecture

The aircraft is designed for cost-effective rapid manufacturing and assembly. Additive manufacturing (3D printing) is used to fabricate the aerodynamic surfaces and non-structural components using lightweight PLA (LW-PLA), while stronger PLA+ is used for structural parts. The fuselage consists of four carbon fiber tubes joined by PLA+ ribs, forming a box frame that supports the empennage, wing mount, and aerodynamic skin. The wings feature two carbon fiber spars (0.82" and 0.32" diameter), with LW-PLA segments and hinged control surfaces actuated by servos via metal pushrods. Square carbon fiber tubes form the booms, and bent aluminum bars and rods serve as landing gear struts, fitted with aluminum wheels and rubber tires. Servos, gears, and avionics are off-the-shelf components.

FLIGHT CONTROL ARCHITECTURE

The top-level FCS architecture is shown in Fig. 2. The FCS can operate in TCS or TMS **control modes** and in VTOL or CTOL **operating modes**. The speed envelope is divided into the following distinct **flight modes**:

- Hybrid Flight Mode (HFM): In HFM, the weight of the aircraft is borne by a combination of thrust and aerodynamic lift, with the contribution of the latter increasing with airspeed. This mode includes hover.
- Transition Flight Mode (TFM): This transient flight mode involves the conversion between hybrid and forward flight modes during acceleration (departure transition) and deceleration (arrival transition).
- Forward Flight Mode (FFM): In FFM, weight is supported entirely by aerodynamic lift. Nacelles are in horizontal position and lift propulsors are inactive.

In prior work, an additional flight mode, Vertical Flight Mode (VFM), applied to hover and low speed translation. In VFM, nacelles were kept fixed in vertical (hover) orientation and fore/aft accelerations were achieved by changing pitch attitude. As the aircraft accelerated, the FCS shifted to HFM, where pitch attitude was set to zero (level deck) and nacelle angle was used to control acceleration.

In the current work, VFM is suppressed and in VTOL operating mode, the aircraft takes off and lands vertically while in HFM. This choice allows better position-keeping at hover (especially in windy conditions) by changing nacelle angle rather than changing pitch attitude, which requires overcoming the aircraft pitching moment of inertia by changing RPM N_2, N_3, N_5, N_6, which in turn requires propeller and motor inertia to be overcome first.

Inceptors and Response Types

The inceptors mounted in the GCS, shown in Fig. 3, provide lateral (δ_{lat}), heave (δ_{ver}), directional (δ_{dir}), and speed (δ_{spd}) inputs to the FCS. Each of these is a normalized signal in the $[-1, +1]$ range.

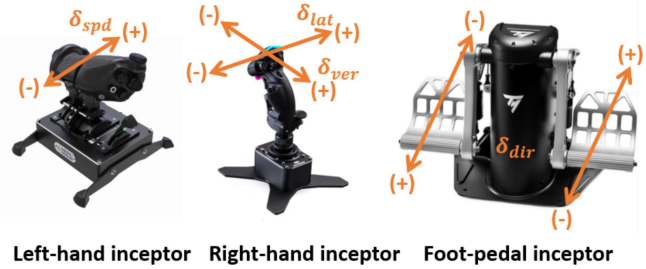

Figure 3. VT-03-s Shadow inceptors

The single-axis left-hand inceptor (LHI) is used to control airspeed. The commands generated by the LHI in TCS and TMS control modes are summarized in Fig. 4. With

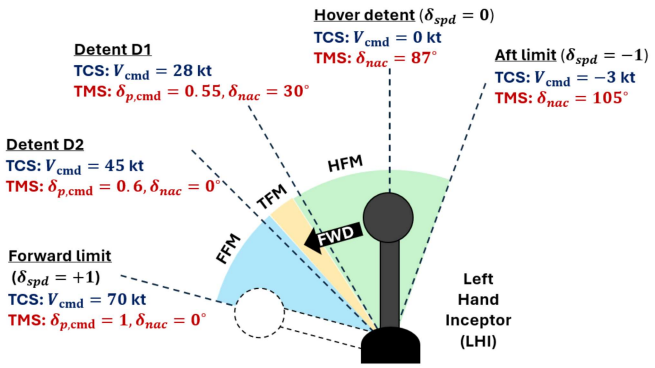

Figure 4. Left-hand inceptor logic

both schemes, LHI inputs control transitions between flight modes. With TCS active, the LHI input generates a commanded speed V_{cmd}, which is used to generate a normalized acceleration command as $(\dot{V}/g)_{\text{cmd}} = K_v(V_{\text{cmd}} - V)$ in all flight modes. With TMS active, the LHI input generates a nacelle position command $\delta_{nac,\text{cmd}}$ and a main propulsor power setting command $\delta_{p,\text{cmd}}$ in FFM.

When at the aft limit ($\delta_{spd} = -1$), in TCS, the maximum aft velocity of −3 kt is commanded, while in TMS, the nacelles are commanded to their upper limit of 105°. When at the hover detent, in TCS, zero speed is commanded while in TMS, the nacelles are commanded to an 87° angle (approximate hover setting). With TCS active, detent D1 commands a speed of 28 kt, while with TMS active, the nacelles are commanded to a 30° deflection, with main propulsors set to 55% power. In detent D2, TCS commands 45 kt airspeed, while TMS commands the nacelles to 0% (forward flight position) and sets main propulsors to 60% power. At the forward limit, TCS commands the maximum speed of 70 kt, while in TMS, the main propulsors are set to 100% power.

Starting from hover, placing the LHI into detent D2 causes the vehicle to accelerate to forward flight in both TCS and TMS control modes. From forward flight, placing the LHI in detent D1 causes the aircraft to decelerate to HFM with both TCS and TMS control modes.

Fore/aft movements of the two-axis right-hand inceptor (RHI) generate the δ_{ver} input. In TCS control mode, this commands vertical velocity $\dot{h}_{\text{cmd}}$ in all flight modes. When in HFM in TMS control mode, the δ_{ver} input generates an incremental normalized vertical thrust command $\Delta(T/W)_{\text{cmd},V}$. When in TFM or FFM in TMS control mode, the δ_{ver} input generates a proportional incremental normal load factor $\Delta n_{z,\text{cmd}}$, which is then translated into a corresponding speed-dependent pitch rate command q_{cmd} through the relationship $q_{\text{cmd}} = (g/V_\infty)\Delta n_{z,\text{cmd}}$.

Left/right movements of the RHI generate the δ_{lat} input. In TCS control mode, this generates a proportionate bank angle command ϕ_{cmd}. The bank command limit is 15° below 10 kt and 45° at higher speeds. Below 10 kt, when the inceptor is centered ($\delta_{lat} = 0$), any lateral velocity is dissipated by automatically generating an opposite bank command. Above 10 kt, lateral inputs also generate a yaw rate command component for turn coordination, $r_{\text{cmd},tc} = (g/V_\infty)\sin(\phi_{\text{cmd}})$, and a pitch rate command component for turn compensation, $q_{\text{cmd},tc} = (g/V_\infty)\tan(\phi_{\text{cmd}})\sin(\phi_{\text{cmd}})$.

With TMS active, lateral inputs δ_{lat} below 10 kt generate bank commands in the same way as for TCS in this speed range. At higher speeds, lateral inputs generate a proportionate roll rate command p_{cmd}. The turn coordination yaw rate component $r_{\text{cmd},tc}$ and turn compensation pitch rate component $q_{\text{cmd},tc}$ are only applied when $|\phi| \le 60°$ and $|p_{\text{cmd}}| \le 40°/s$ so as not to inadvertently interfere with intended aggressive maneuvering.

The foot-pedal inceptor (FPI) is used to generate the δ_{dir} input. In TCS control mode, this input generates a proportionate yaw rate command r_{cmd} in all flight modes, which is added to the turn coordination component $r_{\text{cmd},tc}$ to yield the final yaw rate command. With TMS active, there is a direct feed-through of the pedal input δ_{dir} in addition to the $r_{\text{cmd},tc}$ component.

Holds (Pilot Relief Functions)

The holds available in TCS and TMS flight modes are summarized in Table 3. The holds engage/disengage automatically based on inceptor position and aircraft state.

In TCS mode, the altitude hold (ALT HOLD) function engages when $\delta_{ver} = 0$ and maintains the current altitude through a $\dot{h}_{cmd}$ generated by proportional-integral (PI) control action on the altitude error. Any non-zero δ_{ver} input disengages the hold. The heading hold (HDG HOLD) function engages below 10 kt when $\delta_{dir} = 0$ and generates r_{cmd} to maintain the current heading. It disengages with any non-zero pedal input. The track hold (TRK HOLD) function engages above 10 kt when lateral input $\delta_{lat} = 0$ and generates bank angle and yaw rate commands to maintain the current ground track. It disengages with any non-zero lateral input. The position hold (POSN HOLD) function engages at low speeds when $\delta_{lat} = 0$ and $\delta_{spd} = 0$ and maintains current position by generating bank ϕ_{cmd} and acceleration $(\dot{V}/g)_{\text{cmd}}$ commands. It disengages if there is any non-zero δ_{lat} or δ_{spd} input.

In TMS mode, the BANK HOLD function engages if $\delta_{lat} = 0$ above 10 kt and within the attitude envelope

Table 3. Summary of TCS and TMS holds

Hold	Description	Cmd Generated
	TCS holds	
ALT HOLD	Altitude hold	$\dot{h}_{\text{cmd}}$
HDG HOLD	Heading hold	r_{cmd}
TRK HOLD	Track hold	$\phi_{\text{cmd}}, r_{\text{cmd}}$
POSN HOLD	Position hold	$(\dot{V}/g)_{\text{cmd}}, \phi_{\text{cmd}}$
	TMS holds	
BANK HOLD	Bank angle hold	p_{cmd}
FPA HOLD	Flightpath hold	q_{cmd}

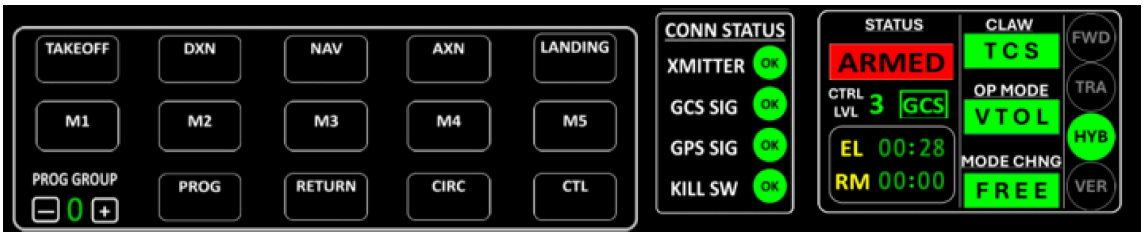

Figure 5. Auto-flight and mode selector touchscreen panel in GCS

$|\phi| \leq 60°, |\theta| \leq 30°$ and holds the current bank angle by generating roll rate command p_{cmd}. It disengages with any non-zero lateral input. The flightpath angle hold (FPA HOLD) function engages in TFM and FFM and maintains the current FPA γ if $\delta_{ver} = 0$ while within the attitude/trajectory envelope $|\phi| \leq 60°, |\theta| \leq 30°, |\gamma| \leq 10°$. It generates a pitch rate command q_{cmd} and disengages if there is a non-zero δ_{ver} input.

Automatic Flight Functions and Mode Selection

The pilot can engage/disengage automatic flight (auto-flight) functions using a touchscreen panel on the GCS, shown in Fig. 5. These are only available in TCS control mode. Auto-flight functions are distinct from holds in that unlike holds, they have to be engaged by the pilot. The following functions are available at the time of writing:

- TAKEOFF: If engaged in VTOL mode, it generates $\dot{h}_{\text{cmd}}$ to lift off from the ground and level off at a pre-set altitude (around 20 ft). If engaged in CTOL mode, it sets a safe speed command for wingborne flight, generates $\dot{h}_{\text{cmd}}$ to induce takeoff rotation, climb to, and level off at a pre-set height above the runway. It does not provide any lateral path guidance.

- CTL (centerline track): Above 10 kt in-flight, this function generates coordinated bank and yaw rate commands to track a defined runway centerline. Below 10 kt, bank is commanded to track centerline, while yaw rate is commanded to align with runway heading. This function is also available in CTOL mode on the ground, where it generates yaw rate commands to taxi along the centerline. The steering algorithm continuously calculates cross-track error (CTE) and attempts to drive it to zero. It does not provide any vertical path guidance.

- NAV (navigation): The navigation function guides the aircraft along a predefined set of waypoints (selected using buttons M1-M5), providing both lateral and vertical path guidance. It uses the same lateral steering algorithm as CTL, but with a turn anticipation function. The NAV function can also invoke TAKEOFF, LANDING, CIRC, and CTL functions when necessary.

- CIRC (circle): This function tracks a constant-radius circle while compensating for prevailing winds. The turn direction, circle center, and turn radius are captured when the pilot banks in the intended direction and engages the function. This function does not provide any vertical path guidance.

- LANDING: When engaged in CTOL mode, the aircraft descends at a pre-set flightpath angle. As it approaches the ground, the flightpath angle becomes shallower, resulting in a roundout and landing flare. When engaged in VTOL mode, the aircraft descends at a pre-set descent rate whose magnitude reduces linearly with height above the ground to a pre-set touchdown vertical velocity. This function does not provide any lateral path guidance.

- RETURN: This function brings the aircraft back to land along a specified trajectory. It can be engaged by the pilot and engages automatically if communication with the GCS is lost.

- PROG (programmed maneuvers): User-defined programmed maneuver sequences can be selected and engaged using the PROG button, the PROG GROUP index, and buttons M1-M5. These are most often used to execute test inputs for system identification.

- DXN (departure transition) and AXN (arrival transition): DXN generates a speed command sufficient for wingborne flight, while AXN decelerates the aircraft back to hover. These legacy functions are redundant for VT-03-s Shadow, where the pilot can set desired speed by simply moving the speed inceptor (δ_{spd}).

Figure 5 also shows how the pilot can toggle the control mode between TCS and TMS and the operating mode between VTOL and CTOL. Toggles between VTOL and CTOL operating modes are only possible on the ground or while in-flight in FFM. The pilot can also select whether changes between flight modes HFM, TFM, and FFM are enabled (FREE) or disabled (LOCKED).

Command Generation Summary

To summarize, the four inceptors, holds, and auto-flight functions can generate the following possible commands

for the downstream MCS (comprising TCS and TMS control architectures) and inner-loops (see Fig. 2):

$$\begin{aligned}
\xi_{H,\text{cmd}} &= \{(\dot{V}/g)_{\text{cmd}},\ \delta_{nac,\text{cmd}},\ \delta_{p,\text{cmd}}\} \\
\xi_{V,\text{cmd}} &= \{\dot{h}_{\text{cmd}},\ \Delta(T/W)_{\text{cmd},V},\ q_{\text{cmd}}\} \\
\xi_{lat,\text{cmd}} &= \{\phi_{\text{cmd}},\ p_{\text{cmd}}\} \\
\xi_{lon,\text{cmd}} &= \{\theta_{\text{cmd}},\ q_{\text{cmd}}\} \\
\xi_{dir,\text{cmd}} &= \{r_{\text{cmd}},\ \delta_{dir}\}
\end{aligned}$$

Maneuver Control System (MCS):

The MCS comprises TCS and TMS, only one of which is active at a time. The behavior of both algorithms in VFM, TFM, and FFM flight modes is described subsequently.

Fundamental TCS Calculations: For the TCS algorithm, the error between commanded and actual normalized acceleration is computed as

$$n_{\text{cmd},H} = \left(\frac{\dot{V}}{g}\right)_{\text{cmd}}, \qquad n_H = \left(\frac{\dot{V}}{g}\right),$$
$$e_{n_H} = n_{\text{cmd},H} - n_H = \left(\frac{\dot{V}}{g}\right)_{\text{cmd}} - \left(\frac{\dot{V}}{g}\right)$$

The error between commanded and actual vertical velocity is converted to an analogous normalized acceleration error through a factor τ_V as

$$n_{\text{cmd},V} = \frac{\dot{h}_{\text{cmd}}}{g\tau_V}, \qquad n_V = \frac{\dot{h}}{g\tau_V},$$
$$e_{n_V} = n_{\text{cmd},V} - n_V = \frac{\dot{h}_{\text{cmd}} - \dot{h}}{g\tau_V} \tag{1}$$

Normalized thrust components in the horizontal and vertical directions are then obtained through proportional-integral (PI) control action as

$$(T/W)_{\text{cmd},H} = K_{IH}\int e_{n_H}\,dt - K_{PH}\,n_H,$$
$$(T/W)_{\text{cmd},V} = K_{IV}\int e_{n_V}\,dt - K_{PV}\,n_V \tag{2}$$

The integral action (with gains K_{IH}, K_{IV}) attempts to zero out errors e_{n_H} and e_{n_V}. The proportional term (with gains K_{PH}, K_{PV}) provide damping.

For the VT-03-s Shadow configuration, under the assumption of equal thrust share among all six propulsors in hover, main and lift propulsor thrust share parameters are defined as $\zeta_{mp} = 4/6$, $\zeta_{lp} = 2/6$.

Since only the main propulsors can tilt and provide both horizontal and vertical components of thrust, the Thrust Axis Inclination (TAI) is defined as

$$\theta_{TAI} = \tan^{-1}\left\{\frac{\zeta_{mp}(T/W)_{\text{cmd},V}}{(T/W)_{\text{cmd},H}}\right\} \tag{3}$$

TCS Logic in HFM: The nacelle, thrust, and pitch targets are computed as

$$\delta^*_{nac,\text{cmd}} = \theta_{TAI} \tag{4}$$
$$(T/W)^*_{mp,\text{cmd}} = \sqrt{(T/W)^2_{\text{cmd},H} + \{\zeta_{mp}(T/W)_{\text{cmd},V}\}^2} \tag{5}$$
$$(T/W)^*_{lp,\text{cmd}} = \zeta_{lp}(T/W)_{\text{cmd},V} \tag{6}$$
$$\theta^*_{\text{cmd}} = \theta_{TAI} - \delta^{max}_{nac}, \quad 0 \le \theta_{\text{cmd}} \le 5^\circ \tag{7}$$

Rate commands for each of the above are generated as $\dot{X} = (X^* - X)/\tau$, to achieve the targets with first-order dynamics. Thrust changes are synchronized with nacelle angle changes (taking into account the nacelle actuator rate limit, which is set to $\pm 15^\circ/s$) to ensure that thrust and nacelle targets are reached simultaneously.

The pitch command remains zero (level deck) unless the nacelles have reached their upper limit, in which case up to 5° of pitch-up is permitted to aid deceleration.

In HFM, the nacelles are limited to $\delta_{nac,\text{cmd}} \in [30^\circ, 105^\circ]$. Lift propulsor thrust is lower-limited to $(T/W)^*_{lp,\text{cmd}} \ge 0.1$ to prevent unintended shutdown while in HFM.

TMS Logic in HFM: The nacelle angle command generated by the LHI position is achieved subject to nacelle actuator rate limits. The pitch command is set to zero.

The vertical component of thrust is computed based on the $\Delta(T/W)_{\text{cmd}}$ from the RHI fore/aft input as

$$\begin{aligned}
(T/W)_{\text{cmd},V} &= \Delta(T/W)_{\text{cmd},V} + (T/W)_{trim} - K_{PV}\,n_V \\
\frac{d}{dt}(T/W)_{trim} &= -K_{IV}\,n_V \qquad \text{if } \Delta(T/W)_{\text{cmd},V} = 0 \\
&= 0 \qquad\qquad\ \text{if } \Delta(T/W)_{\text{cmd},V} \neq 0
\end{aligned} \tag{8}$$

The main and lift propulsor thrust targets (attained through first-order dynamics as before) are computed as:

$$\begin{aligned}
(T/W)^*_{mp,\text{cmd}} &= \frac{\zeta_{mp}\,(T/W)_{\text{cmd},V}}{\sin(\delta_{nac})} \\
(T/W)^*_{lp,\text{cmd}} &= \zeta_{lp}(T/W)_{\text{cmd},V}
\end{aligned} \tag{9}$$

The term containing proportional gain K_{PV} provides a damping effect at all times. The integral action through gain K_{IV} adjusts the trim thrust value $(T/W)_{trim}$ when $\delta_{ver} = 0$, i.e., $\Delta(T/W)_{\text{cmd},V} = 0$. The net control action maintains zero vertical velocity ($n_V = 0$) when $\delta_{ver} = 0$.

TCS Logic in TFM: When accelerating through TFM, the TCS pitch and main propulsor thrust control logic are identical to those described subsequently under TCS logic in FFM. The lift propulsor thrust command is reduced to zero at a constant specified rate. The nacelle rate (limited to $\pm 6^\circ/s$ in TFM) is synchronized with this such that nacelles reach forward flight position approximately when the lift propulsor thrust command reduces to zero.

When decelerating through TFM, the vertical thrust command $(T/W)_{\text{cmd},V}$ is increased at a constant specified rate while the horizontal thrust command is set to $(T/W)_{\text{cmd},H} = 0.3$. The TAI is then computed per Eq. 3. The nacelle and thrust targets are then computed per Eq. 4-6 and achieved (as before) via synchronized first-order dynamics. The pitch control logic is identical to that described subsequently for FFM.

TMS Logic in TFM: The nacelle angle command generated by the LHI position is achieved subject to a lower nacelle actuator rate limit of $\pm 6°/s$ in TFM.

The lift propulsor thrust target is set through linear interpolation based on nacelle position and reference values of 0.3 at 30° nacelle angle and 0 at forward nacelle position.

The main propulsor power setting command is generated through linear interpolation based on nacelle position and the reference values at detents D1 and D2 (Fig. 4).

The logic for main propulsor thrust control and control about the pitch axis are identical to those described subsequently under TMS logic in FFM.

TCS Logic in FFM: Nacelles are commanded to their forward flight position. Lift propulsors are deactivated. The main propulsor thrust control law is

$$\begin{aligned}(T/W)_{mp,\text{cmd}} &= K_{IH}\int \{e_{n_H} + F(\dot{h}_{\text{cmd}} - \dot{h})\}\, dt \\ &- K_{PH}\{n_H + F\dot{h}\} \end{aligned} \tag{10}$$

This control action responds to both acceleration and vertical velocity commands. The integral action attempts to drive the errors of commanded acceleration and height rate to zero. The proportional term adds damping.

The pitch control action is the summation of several contributory terms:

$$\begin{aligned}\theta_{\text{cmd}} &= \theta_{\text{cmd},1} + \theta_{\text{cmd},2} + \theta_{\text{cmd},3} + \theta_{\text{cmd},4} + \theta_{\text{cmd},5} \\ \theta_{\text{cmd},1} &= (1-k_{SP})\, K_{IV} F \int (\dot{h}_{\text{cmd}} - \dot{h})\, dt - K_{PV} F \dot{h} \\ \theta_{\text{cmd},2} &= k_{SP}\left[K_{IH}\int e_{n_H}\, dt - K_{PH} n_H\right] \\ \theta_{\text{cmd},3} &= -K_{trim}\, n_H \\ \theta_{\text{cmd},4} &= \int \dot{\theta}^*_{\text{cmd}}\, dt \\ \theta_{\text{cmd},5} &= K_\theta^{ff} n_V \end{aligned} \tag{11}$$

Under nominal conditions, when the propulsion system power setting is not at maximum ($\delta_p = 1$) or minimum ($\delta_p = 0$) limits, $k_{SP} = 0$, and the TCS logic tracks both acceleration and vertical velocity commands. If either limit is reached, it is necessary to prioritize tracking of either the acceleration command (speed priority, $k_{SP} = 1$) or the height rate command (path priority, $k_{SP} = 0$).

The $\theta_{\text{cmd},1}$ term tracks the commanded height rate. The factor F is computed as $F = 1/V$. If speed priority is active ($k_{SP} = 1$), the integral term is nullified.

The $\theta_{\text{cmd},2}$ term contributes if speed priority is active ($k_{SP} = 1$). The integral action attempts to zero out acceleration error e_{n_H}. The proportional term adds damping.

The $\theta_{\text{cmd},3}$ term attempts to balance aerodynamic lift and weight through a nose-down pitch attitude change (reducing angle of attack) with increasing airspeed through gain $K_{trim}(V) = 4g(W/S)/\left(\rho V^3 C_{L_\alpha}\right)$, where W/S is the wing loading, ρ is the density, and C_{L_α} is the lift-curve slope.

The $\theta_{\text{cmd},4}$ term changes the pitch command at a specified rate. It is only used to induce takeoff rotation in CTOL operating mode.

The $\theta_{\text{cmd},5}$ term is a feed-forward control component that is proportional to vertical velocity command and quickens the net pitch response of the aircraft.

TMS Logic in FFM: Nacelles are commanded to their forward flight position. Lift propulsors are deactivated. Main propulsor thrust command is varied with a first-order dynamic to achieve the desired power setting command $\delta_{p,\text{cmd}}$.

$$\frac{d}{dt}(T/W)_{mp,\text{cmd}} = \frac{\delta_{p,\text{cmd}} - \delta_p}{\tau_{\delta_p}} \tag{12}$$

The pitch rate command q_{cmd} generated from upstream is propagated, and the pitch command θ_{cmd} is set to track the actual pitch attitude θ'.

Flight Mode Transition Logic: The criteria that must be met for flight mode transitions with TCS and TMS active are summarized in Table 4. The command quantities involved, V_{cmd} for TCS and $\delta_{nac,\text{cmd}}$ for TMS, are set solely using the LHI. With only one exception, flight mode transitions in TMS depend only on nacelle commanded and actual position. The exception is the FFM → TFM transition, which also involves airspeed falling below a threshold as one of the criteria. All flight mode transitions with TCS active involve a criterion on commanded speed.

Table 4. Flight mode transition logic

From → To	Criterion	TCS	TMS
HFM → TFM	$V_{\text{cmd}} > 40$ kt	✓	
	$\delta_{nac} \le 30°$	✓	✓
TFM → FFM	$V_{\text{cmd}} > 40$ kt	✓	
	$\delta_{nac} \le 7°$	✓	✓
	$\delta_{nac,\text{cmd}} \le 1°$		✓
FFM → TFM	$V_{\text{cmd}} < 30$ kt	✓	
	$V < 39$ kt	✓	
	$V < 40$ kt		✓
	$\delta_{nac,\text{cmd}} \ge 7°$		✓
TFM → HFM	$V_{\text{cmd}} < 30$ kt	✓	
	$\delta_{nac} > 30°$	✓	✓

Explicit Model-Following (EMF) Inner-Loops:

The inner-loop EMF control system, illustrated in Fig. 6, produces normalized roll, pitch, and yaw control efforts, denoted as $u_{lat}, u_{lon}, u_{dir} \in [-1, +1]$, respectively. The implementation follows Ref. 14.

The upstream command X_{cmd} passes through the *command model* (CM), which generates attitude and rate commands (respectively, $X_{CM}, \dot{X}_{CM}$) based on first or second-order command model transfer functions (CMTF). An *inverse plant* generates a feed-forward control component $u^{ff}_{(\cdot)}$ based on a lower order equivalent system (LOES) model of the on-axis aircraft dynamics ($p/u_{lat}, q/u_{lon}$, and r/u_{dir} for roll, pitch, and yaw axes respectively) to approximately follow the commanded attitude or rate. A *feedback controller* uses classical proportional-integral-derivative (PID) control action based on sensor feedback $Y_1^{'}$ and $Y_2^{'}$ of attitude Y_1 and rate Y_2 to generate a feedback control component $u^{fb}_{(\cdot)}$ to stabilize unstable dynamics, provide robustness and gust/turbulence rejection, and compensate for the approximate nature of the LOES. The CM outputs are passed through an *equivalent delay* to synchronize them with the feedback signals, compensate for delays/lags in the plant and sensor dynamics, and avoid over-driving actuators.

The default operation (with TCS active) involves attitude command tracking for roll and pitch axes, and rate command tracking for yaw axis. With TMS active, the roll axis switches to rate command tracking above 10 kt, and the pitch axis does so in TFM and FFM.

Roll axis: A first-order LOES is used over the entire speed envelope to compute the feed-forward control u^{ff}_{lat}:

$$\frac{p}{u_{lat}}(s) = \frac{L_{u_{lat}}}{s - L_p} \Rightarrow u^{ff}_{lat}(t) = \frac{1}{L_{u_{lat}}} \left\{ \dot{p}_{CM}(t) - L_p \; p_{CM}(t) \right\}$$

When tracking a commanded bank angle ϕ_{cmd}, the second-order CMTF is given by

$$\frac{\phi_{CM}}{\phi_{\text{cmd}}}(s) = \frac{\omega^2_{CM}}{s^2 + 2\zeta_{CM}\omega_{CM} s + \omega^2_{CM}} \tag{13}$$

and is solved as the equivalent time-domain model

$$\begin{bmatrix} \dot{\phi}_{CM} \\ \dot{p}_{CM} \end{bmatrix} = \begin{bmatrix} 0 & 1 \\ -\omega^2_{CM} & -2\zeta_{CM}\,\omega_{CM} \end{bmatrix} \begin{bmatrix} \phi_{CM} \\ p_{CM} \end{bmatrix} + \begin{bmatrix} 0 \\ \omega^2_{CM} \end{bmatrix} \phi_{\text{cmd}} \tag{14}$$

The feedback component $u^{fb}_{lat}(t)$ is formed by PID action on errors of bank, $e_\phi(t) = \phi'_{CM}(t) - \phi'(t)$, and roll rate, $e_p(t) = p'_{CM}(t) - p'(t)$ as

$$\begin{aligned} u^{fb}_{lat}(t) &= K_\phi \; e_\phi(t) + K_p \; e_p(t) + u^{trim}_{lat}(t), \\ u^{trim}_{lat}(t) &= K_{I\phi} \int e_\phi(t) \cdot dt \end{aligned} \tag{15}$$

When tracking a commanded roll rate p_{cmd}, p_{CM} is related to p_{cmd} through a first order time constant τ_p while ϕ_{CM} tracks bank feedback ϕ' as

$$\dot{\phi}_{CM} = \frac{\phi' - \phi_{CM}}{\tau_\phi}, \qquad \dot{p}_{CM} = \frac{p_{\text{cmd}} - q_{CM}}{\tau_p} \tag{16}$$

The feedback component is generated as

$$\begin{aligned} u^{fb}_{lat}(t) &= K_p \; e_p(t) + u^{trim}_{lat}(t), \\ u^{trim}_{lat}(t) &= K_{Ip} \int e_p(t) \cdot dt \end{aligned} \tag{17}$$

The integral action in Eq. 17 is only performed when $|p_{\text{cmd}}|$ lies below a threshold. The net roll control effort is $u_{lat}(t) = u^{ff}_{lat}(t) + u^{fb}_{lat}(t)$.

Pitch axis: The feed-forward control u^{ff}_{lon} blends from first-order at hover and low speeds to second-order at higher speeds. The form and solution of the first-order case are as follows:

$$\frac{q}{u_{lon}}(s) = \frac{M_{u_{lon}}}{s - M_q} \implies u^{ff}_{lon}(t) = \frac{1}{M_{u_{lon}}} \left\{ \dot{q}_{CM}(t) - M_q \; q_{CM}(t) \right\} \tag{18}$$

The form of the second-order LOES is

$$\frac{q}{u_{lon}}(s) = \frac{M_{u_{lon}} \left(s + 1/T_{\theta_2} \right)}{s^2 + 2\zeta_{sp}\omega_{sp} s + \omega^2_{sp}}, \tag{19}$$

where ζ_{sp} and ω_{sp} are respectively the damping ratio and natural frequency of the aircraft short period mode. The LOES is solved in the time-domain to obtain

$$\begin{aligned} \dot{u}^{ff}_{lon}(t) = \frac{1}{M_{u_{lon}}} \Big\{ & \ddot{q}_{CM}(t) + 2\zeta_{sp}\omega_{sp} \; \dot{q}_{CM}(t) + \omega^2_{sp} \; q_{CM}(t) \\ & - \frac{M_{u_{lon}}}{T_{\theta_2}} \; u^{ff}_{lon}(t) \Big\} \end{aligned} \tag{20}$$

When a pitch attitude command θ_{cmd} is tracked, the second-order CMTF is analogous to that for the roll axis, with $\phi_{CM}, p_{CM}, \phi_{\text{cmd}}$ replaced by $\theta_{CM}, q_{CM}, \theta_{\text{cmd}}$ in Eq. 14. The pitch rate component for turn compensation, $q_{\text{cmd},tc}$ is added to the q_{CM} solution to allow the rate command component to propagate even when the system is tracking pitch attitude.

The feedback component u^{fb}_{lon} is generated through PID control action on errors of pitch attitude, $e_\theta(t) = \theta'_{CM}(t) - \theta'(t)$, and pitch rate, $e_q(t) = q'_{CM}(t) - q'(t)$ as

$$\begin{aligned} u^{fb}_{lon}(t) &= K_\theta \; e_\theta(t) + K_q \; e_q(t) + u^{trim}_{lon}(t) \\ u^{trim}_{lon}(t) &= K_{I\theta} \int e_\theta(t) \cdot dt \end{aligned} \tag{21}$$

When tracking a commanded pitch rate q_{cmd}, q_{CM} and θ_{CM} are computed as

$$\dot{\theta}_{CM} = \frac{\theta' - \theta_{CM}}{\tau_\theta}, \qquad \dot{q}_{CM} = \frac{q_{\text{cmd}} - q_{CM}}{\tau_q} \tag{22}$$

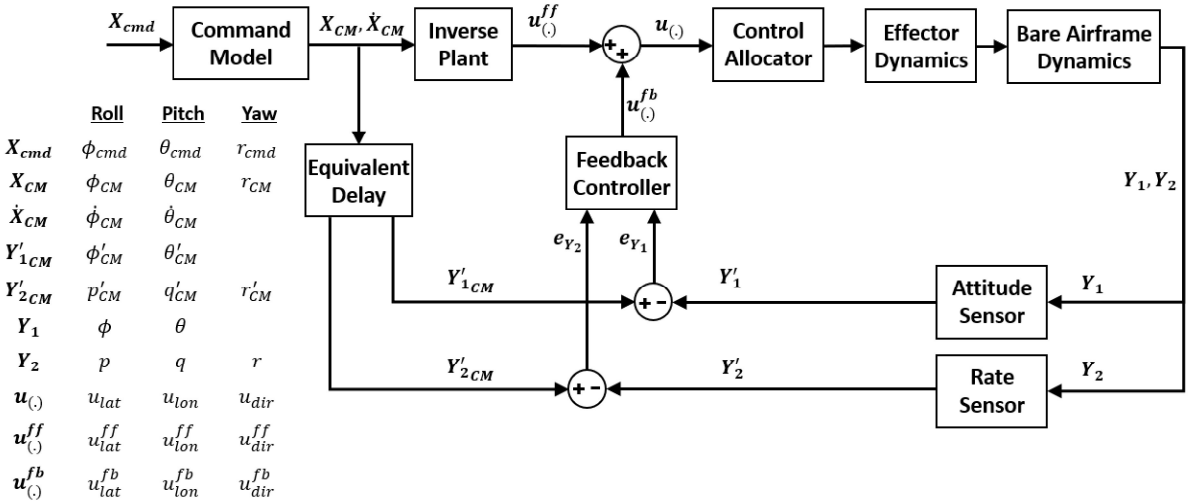

Figure 6. Explicit model-following (EMF) inner-loop control system

The feed-forward component is then generated using Eq. 20. The feedback component is generated as

$$\begin{aligned} u^{fb}_{lon}(t) &= K_q\, e_q(t) + u^{trim}_{lon}(t) \\ u^{trim}_{lon}(t) &= K_{Iq} \int e_q(t) \cdot dt \end{aligned} \tag{23}$$

The net pitch control effort is $u_{lon}(t) = u^{ff}_{lon}(t) + u^{fb}_{lon}(t)$.

At equilibrium steady, wings-level flight at pitch attitude $\theta_{\text{cmd}} = \theta' = \theta_{trim}$ and bank $\phi_{cmd} = \phi' = 0$, the command model solutions are $\theta_{CM} = \theta_{trim}, q_{CM} = 0$ and $\phi_{CM} = 0, p_{CM} = 0$, with higher derivatives equal to zero. The feed-forward components are $u^{ff}_{lon} = 0, u^{ff}_{lat} = 0$ and feedback errors are $e_\theta = e_\phi = 0, e_q = e_p = 0$, and the entirety of the control effort resides in the integral channels, i.e., $u_{lon} = u^{trim}_{lon}, u_{lat} = u^{trim}_{lat}$. This allows transient-free switching between attitude and rate command tracking.

Yaw axis: For the yaw axis, with TCS active, the CM yaw rate command r_{CM} is related to the yaw rate command r_{cmd} through a first-order CMTF

$$\frac{r_{CM}}{r_{\mathbf{cmd}}}(s) = \frac{1}{\tau_{CM} s + 1} \Rightarrow \dot{r}_{CM}(t) = \frac{1}{\tau_{CM}} \{r_{\mathbf{cmd}}(t) - r_{CM}(t)\}. \tag{24}$$

At low VFM speeds, the feed-forward component u^{ff}_{dir} is computed using a first-order LOES as

$$\frac{r}{u_{dir}}(s) = \frac{N_{u_{dir}}}{s - N_r} \Rightarrow u^{ff}_{dir}(t) = \frac{1}{N_{u_{dir}}} \{\dot{r}_{CM}(t) - N_r\, r_{CM}(t)\} \tag{25}$$

At higher speeds and in FFM, the feed-forward component is washed out and only the feedback component u^{fb}_{dir} is retained. This is generated based on yaw rate error, $e_r(t) = r'_{CM}(t) - r'(t)$ through PI control action as

$$u^{fb}_{dir}(t) = K_r e_r(t) + K_{Ir} \int e_r(t)\, dt \tag{26}$$

When TMS is active, the feed-forward component of Eq. 25 is replaced with a one-to-one component $u^{ff}_{dir} = \delta_{dir}$ based on the pilot's pedal input to the FPI.

Differential Thrust Ground Steering

Differential rpm ΔN_{DT} between the left propellers N_1, N_2 and right propellers N_3, N_4 is used to generate differential thrust for steering during ground operations. This functionality is only active when the nacelles $\delta_{t_1}, \ldots, \delta_{t_4}$ are fully forward. Pilot pedal input δ_{dir} is shaped by a nonlinear mapping to soften the sensitivity near the center while maintaining full authority at maximum input. Total differential RPM is composed of discrete RPM offsets by the pilot, feedforward component at low speed, and feedback component based on yaw rate tracking error.

Control Allocation

The control allocation logic generates the control vector containing the commanded states of each of the aircraft control effectors (Table 2)

$$\begin{aligned} U^{16\times 1}_{\text{cmd}} = \{&\delta_{f_1}, \delta_{f_2}, \delta_{f_3}, \delta_{f_4}, \delta_s, \delta_r, \delta_{t_1}, \delta_{t_2}, \delta_{t_3}, \delta_{t_4}, \\ &N_1, N_2, N_3, N_4, N_5, N_6\}^T \end{aligned}$$

Main propeller RPM commands are computed as follows:

$$\begin{aligned} \begin{bmatrix} N_1 \\ N_2 \\ N_3 \\ N_4 \end{bmatrix} &= \begin{bmatrix} 1.0 & +1.0 & 0.0 & +1 \\ 1.0 & +1.0 & +1.0 & +1 \\ 1.0 & -1.0 & +1.0 & -1 \\ 1.0 & -1.0 & 0.0 & -1 \end{bmatrix} \begin{bmatrix} N_{0,mp} \\ \Delta N_{\phi,mp} \\ \Delta N_{\theta,mp} \\ \Delta N_{\psi,mp} \end{bmatrix} \\ \Delta N_{\phi,mp} &= \Delta N^{max}_{\phi,mp}\, \zeta_{\phi,mp}\, u_{lat} \\ \Delta N_{\theta,mp} &= \Delta N^{max}_{\theta,mp}\, \zeta_{\theta,mp}\, u_{lon} \\ \Delta N_{\psi,mp} &= \Delta N^{max}_{\psi,mp}\, \zeta_{\psi,mp}\, u_{dir} + \Delta N_{DT} \end{aligned} \tag{27}$$

Lift propeller RPM commands are computed as follows:

$$\begin{bmatrix} N_5 \\ N_6 \end{bmatrix} = \begin{bmatrix} 1.0 & +1.0 & -1.0 \\ 1.0 & -1.0 & -1.0 \end{bmatrix} \begin{bmatrix} N_{0,lp} \\ \Delta N_{\phi,lp} \\ \Delta N_{\theta,lp} \end{bmatrix}$$
$$\Delta N_{\phi,lp} = \Delta N^{max}_{\phi,lp}\, \zeta_{\phi,lp}\, u_{lat}$$
$$\Delta N_{\theta,lp} = \Delta N^{max}_{\theta,lp}\, \zeta_{\theta,lp}\, u_{lon} \tag{28}$$

The nacelle tilt angles are computed as

$$\begin{bmatrix} \delta_{t_1} \\ \delta_{t_2} \\ \delta_{t_3} \\ \delta_{t_4} \end{bmatrix} = \begin{bmatrix} 1.0 & -1.0 \\ 1.0 & 0.0 \\ 1.0 & 0.0 \\ 1.0 & +1.0 \end{bmatrix} \begin{bmatrix} \delta_{nac,\mathrm{cmd}} \\ \Delta\delta_{nac,\psi} \end{bmatrix}$$
$$\Delta\delta_{nac,\psi} = \Delta\delta^{max}_{nac,\psi}\, \zeta_{\psi,nac}\, u_{dir} \tag{29}$$

The flaperon deflections are computed as:

$$\begin{bmatrix} \delta_{f_1} \\ \delta_{f_2} \\ \delta_{f_3} \\ \delta_{f_4} \end{bmatrix} = \begin{bmatrix} +1 \\ +1 \\ -1 \\ -1 \end{bmatrix} \left[\Delta\delta_{f,\phi}\right], \qquad \Delta\delta_{f,\phi} = \Delta\delta^{max,\phi}_{f}\, \zeta_{\phi,f}\, u_{lat} \tag{30}$$

The stabilator and rudder deflections are computed as:

$$\delta_s = -\delta^{max}_s\, u_{lon}$$
$$\delta_r = +\delta^{max}_r\, u_{dir} \tag{31}$$

The computed control surface and nacelle deflections are subject to physical deflection limits. The control allocation relationships in Eqs. 27, 28, 29, 30 contain a number of wash-in/wash-out parameters $\zeta_{(\cdot)}$. These are scheduled with respect to nacelle angle as shown in Table 5.

Table 5. Wash-in wash-out schedules (linear variations between data points)

δ_{nac}	90	80	70	60	50	40	≤30
$\zeta_{\phi,mp}$	1	1	0.50	0	0	0	0
$\zeta_{\theta,mp}$	1	0.83	0.67	0.50	0.33	0.17	0
$\zeta_{\psi,mp}$	0	0	0.11	0.33	0.55	0.78	1
$\zeta_{\phi,lp}$	1	1	1	1	1	1	1
$\zeta_{\theta,lp}$	1	1	1	1	1	1	1
$\zeta_{\phi,f}$	1	1	1	1	1	1	1
$\zeta_{\psi,f}$	1	1	0.50	0	0	0	0
$\zeta_{\psi,nac}$	1	1	0.50	0	0	0	0

SIMULATION AND FLIGHT-TEST SETUP

Dual-Purpose Ground Control Station (GCS)

A high-level overview of the communication architecture between the dual-purpose GCS and the physical vehicle or its simulation model is shown in Fig. 7.

In flight test mode, a first-person view (FPV) camera feed from the aircraft is shown on the top screen. The lower touchscreens are driven by telemetry broadcast back from the vehicle. While the GCS pilot flies using the FPV feed, the pilot monitoring stands beside the GCS maintaining visual line-of-sight with the vehicle and is capable of assuming control via a R/C transmitter in case of a vehicle-GCS communication failure. The flight-test engineer monitors the vehicle states on duplicate displays and can also tune specific controller gains in-flight.

In simulation mode, the GCS is interfaced with the flight simulation model implemented using *Modular Aircraft Dynamics and Control Algorithm Simulation Platform* (MADCASP). The FPV display then shows a rendering of the flight environment using X-Plane Flight Simulator for visualization and terrain elevation feedback.

The GCS inceptors were discussed previously and are shown in Fig. 3. The touchscreen displays are shown in Fig. 8. The auto-flight master control panel (A), shown previously in Fig. 5, allows the engagement/disengagement of auto-flight functions. The map display (B) shows a North-up image of the flight test site at Sharpe Field in Tuskegee, AL with an overlay of the waypoint grid. The connection status display (C) shows the connectivity between the GCS and the aircraft. The primary flight display (D) shows key aircraft states, engagement of holds, and vertical and lateral path deviation indicators if NAV or CTL tracking modes are active. Arm status, the flight timer, the active control mode (CLAW), operational mode (OP MODE), mode change selection (FREE or LOCKED), and current flight mode (VFM, HFM, TFM, or FFM) are displayed in (E). The FCS display (F) shows pilot inceptor inputs and intermediate and final FCS commands (see Fig. 2). The nacelle position indicator (G) shows the position of the tilting nacelles.

MADCASP Flight Simulation Model

The MATLAB/Simulink-based MADCASP flight simulation model allows trim analysis, model linearization, and dynamic stability analysis of both the open-loop (bare airframe) and closed-loop systems, which facilitates controller development. With the GCS in simulation mode, the MADCASP Simulink model is time-marched in real-time using a 4th-order Runge-Kutta scheme with a time-step of 1/60 seconds (60 Hz) to plan, simulate, and de-risk flight test profiles prior to executing them in the field.

The aircraft aero-propulsive model (explained in greater detail in Refs. 15–17) discretizes lifting surfaces into spanwise strips and models their aerodynamic loads using a strip theory approach, with a parametric reduced-order downwash model (Ref. 18) and control surface effects modeled based on the USAF DATCOM (Ref. 19). Fuselage and landing gear loads are computed using force and moment coefficient lookup tables generated using FlightStream®. Propeller loads are calculated using a blade element momentum theory propeller model coupled to a 7-state Pitt-Peters dynamic inflow model with wake distortion effects (Ref. 20), which is calibrated with available propeller manufacturer data.

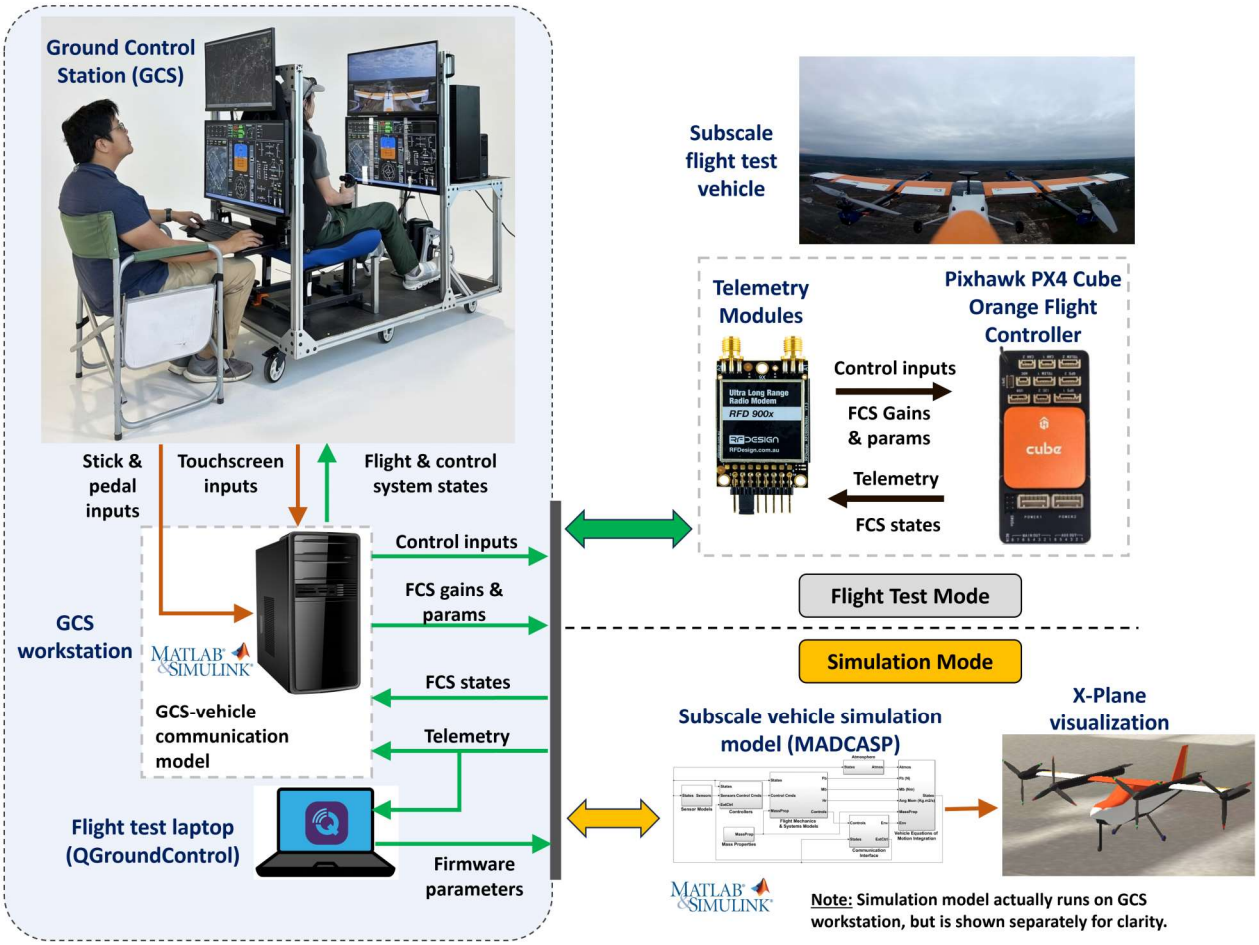

Figure 7. GCS-vehicle and GCS-simulation connectivity

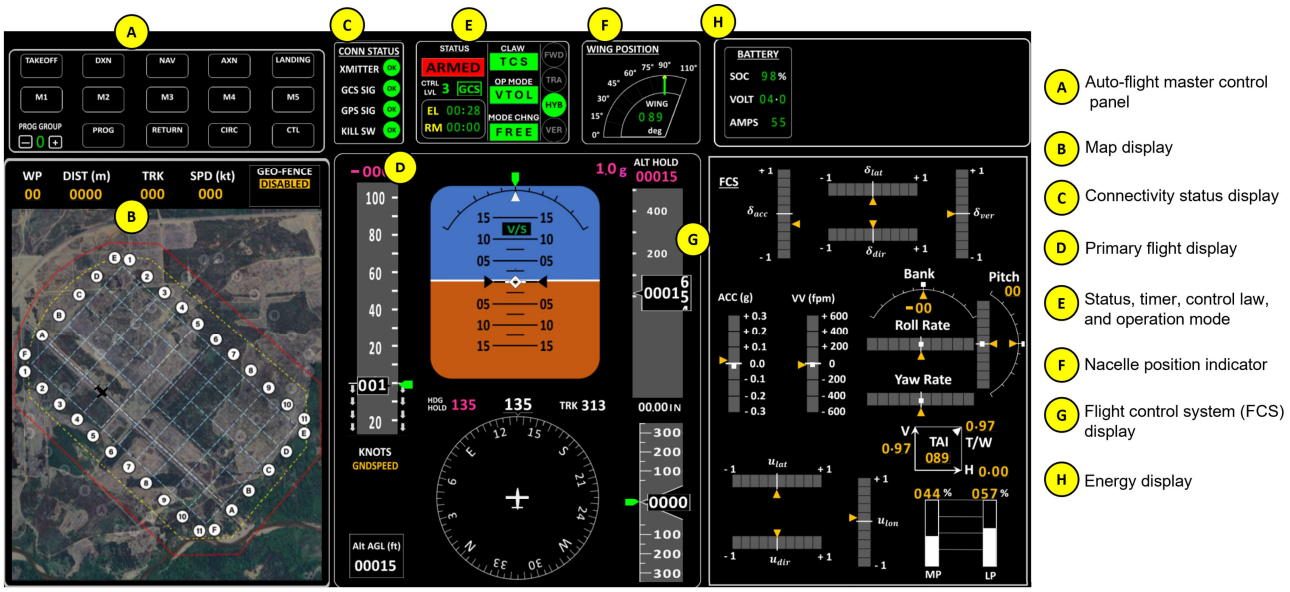

Figure 8. GCS displays for VT-03-s Shadow

FLIGHT TEST RESULTS

Accelerating Transition Using TCS

An accelerating HFM→TFM→FFM transition in TCS control mode is shown in Fig. 9. Onboard and external footage with telemetry overlay is available on YouTube at https://tinyurl.com/TCS-accel.

The acceleration begins from hover at 100 ft above the ground when the speed command is increased to 45 kt. The waypoints programmed into the NAV function require it to track the runway centerline while maintaining 100 ft altitude.

The nacelles begin to tilt forward while the pitch attitude remains level as the aircraft accelerates in HFM. The average rate of nacelle movement during the acceleration to forward flight is approximately $4°/s$.

As the wings generate progressively more lift, the vertical thrust command $(T/W)_{\mathrm{cmd},V}$ (labeled TWV) is seen to decrease. On the other hand, to overcome progressively greater drag, the horizontal thrust command $(T/W)_{\mathrm{cmd},H}$ (labeled TWH) increases. During the acceleration in HFM, the altitude deviation is minimal, only around 10 ft. At t = 15.5 sec, the flight mode shifts into TFM as the HFM→TFM criteria (Table 4) for TCS are met.

In TFM, the lift propulsors are gradually powered down and nose-up pitch command is generated to compensate for the reduction in lift propulsor thrust with an increase in aerodynamic lift. The tradeoff is not perfect, and there is an altitude excursion of +15 ft, corresponding to where the tracking of vertical velocity command is degraded. At t = 22 sec, the flight mode shifts into FFM as the TFM→FFM criteria (Table 4) for TCS are met.

A velocity overshoot is seen to occur during TFM at approximately t = 20 sec. This is partly caused by an increase in aerodynamic efficiency of the airframe as the nacelles get close to their forward flight position. During acceleration, the lateral steering algorithm generated coordinated bank and yaw rate commands to track the runway centerline. The worst cross-track error (CTE) of 4.57 m (20 ft) occurred around 10 kt, above which the lateral steering algorithm performs coordinated turns. Once the aircraft returned to centerline at t = 10 sec, the CTE remained within ±1.70 m (±5.57 ft) thereafter.

Control efforts about roll, pitch, and yaw axes remained relatively low throughout. The only notable trend is the development of nose-down pitch control effort $u_{lon} < 0$ up to around 20 kt airspeed, followed by progressive development of nose-up pitch control effort $u_{lon} > 0$ as the aircraft accelerated into forward flight.

The deficiencies that warrant improvement were the airspeed overshoot and the tracking of vertical velocity during TFM. It is anticipated that these can be improved by further refinement of TCS gains.

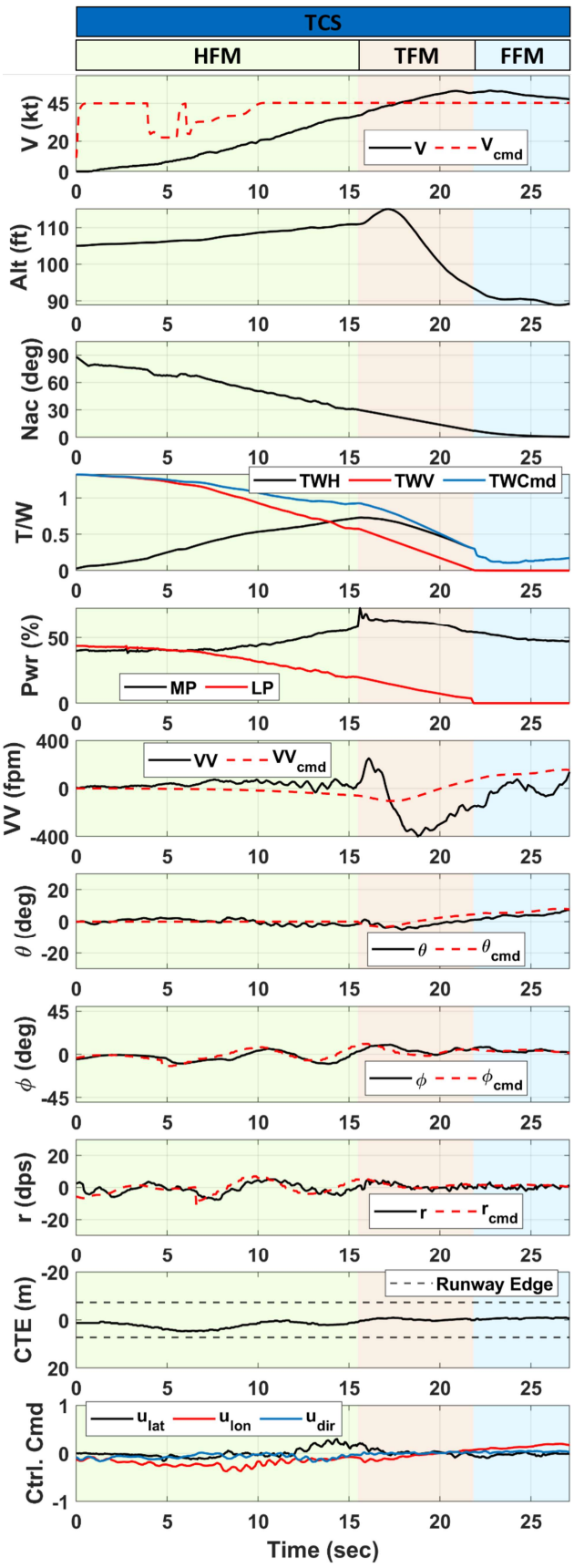

Figure 9. Accelerating transition using TCS

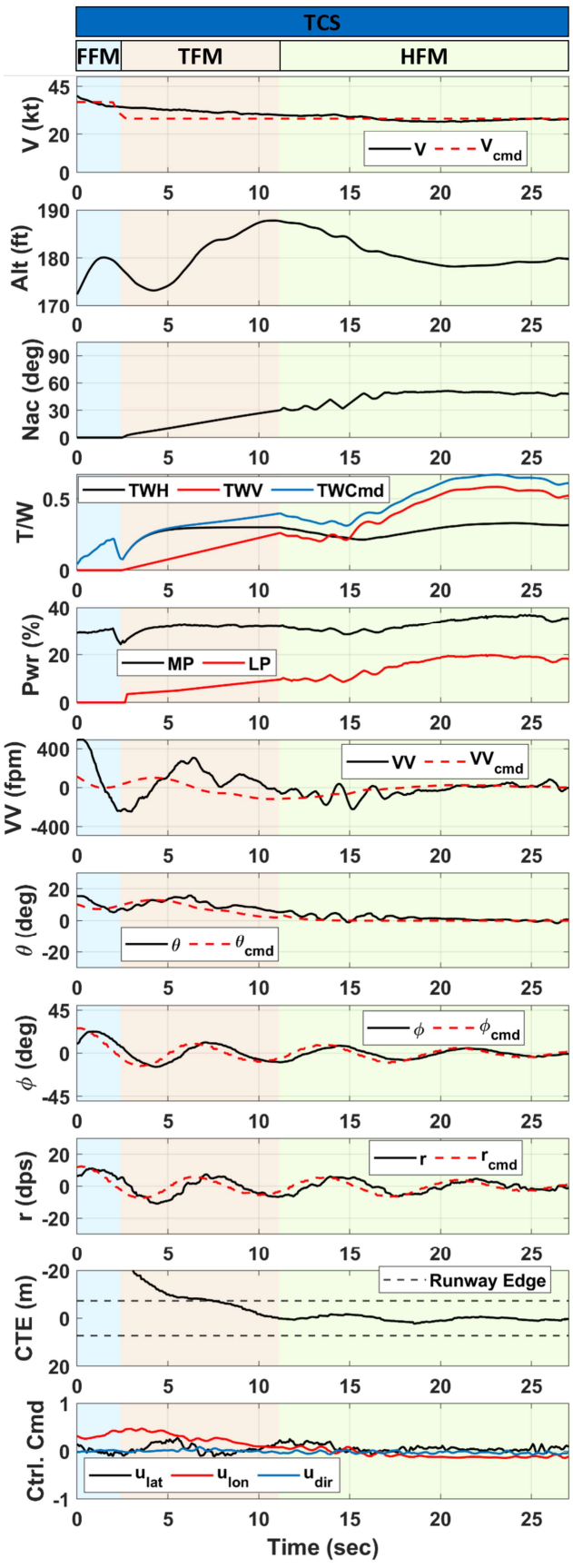

Figure 10. Decelerating transition using TCS

Decelerating Transition Using TCS

A decelerating transition performed using TCS is shown in Fig. 10, which shows deceleration from 35 kt in FFM to 28 kt in HFM. Onboard and external footage with telemetry is available on YouTube at https://tinyurl.com/TCS-decel, which shows the deceleration and subsequent flight until landing. The target altitude during the deceleration shown in Fig. 10 is 180 ft.

At $t = 2$ sec, with the aircraft at 35 kt airspeed, the speed command is reduced to 28 kt. This immediately satisfies the FFM→TFM criteria for TCS (Table 4), which shifts into TFM. In this mode, the nacelles move upward at approximately 3.4°/s while the lift propellers activate and generate progressively more thrust. Vertical flightpath is controlled using pitch attitude.

At t = 11.1 sec, when the nacelles reach 30° angle, the TFM→HFM criteria (Table 4) are met, and TCS shifts into HFM. The pitch attitude command dissipates to zero (level deck), and vertical flightpath is subsequently controlled using the vertical thrust component $(T/W)_{\text{cmd},V}$, shared between the main and lift propulsors. At the end of the interval shown in Fig. 10, the aircraft has slowed to 28 kt, with nacelles at 48° angle, main propulsors at 35% power, and lift propulsors at 18% power.

During the deceleration, the lateral steering algorithm intercepted the runway centerline coming out of a left base-to-final turn. The intercept was complete by the time TCS shifted from TFM to HFM. Thereafter, the CTE remained within ±1.33 m (±4.36 ft).

There was no airspeed undershoot during deceleration. However, similar to acceleration through TFM, the tracking of vertical velocity command during deceleration through TFM warrants further improvement.

Accelerating Transition Using TMS

An accelerating HFM→TFM→FFM transition performed in TMS control mode is shown in Fig. 11. Footage and telemetry of this flight are available on YouTube at https://tinyurl.com/TMS-accel.

Starting from hover at 100 ft altitude in TCS, the control mode was switched to TMS using the touchscreen (Fig. 5). This deactivated TCS-specific altitude hold (ALT HOLD), heading hold (HDG hold), and position hold (POSN HOLD) functions. The control mode change was transient-free. The pilot started the acceleration by commanding forward rotation of the nacelles from 90° to 60° using LHI input, and the aircraft accelerated to approximately 13 kt. The nacelle movement occurred at a 15°/s rate. At t = 14.2 sec, the pilot commanded the nacelles to 52°, causing the aircraft to accelerate up to 24 kt. Thereafter, between t = 20 sec and t = 26 sec, the pilot progressively commanded the nacelles to the forward flight position at an average rate of 7°/s. The aircraft entered TFM

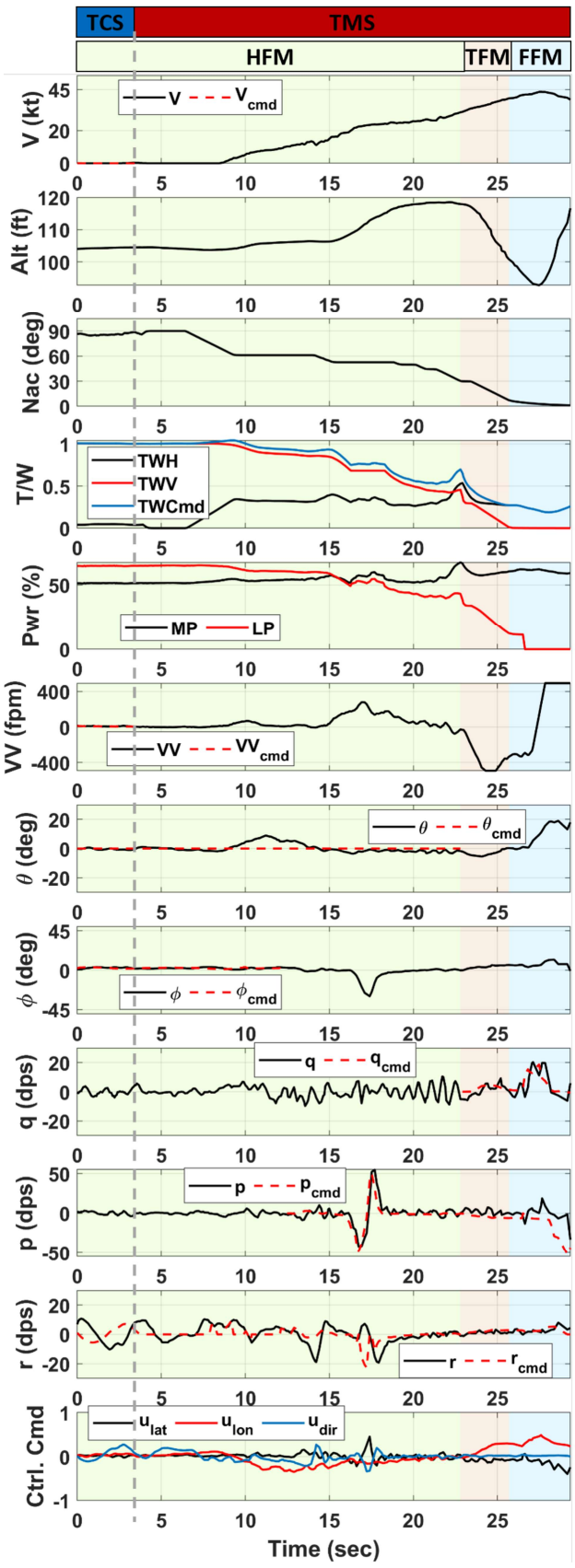

Figure 11. Accelerating transition using TMS

at $t = 22.8$ sec and FFM at $t = 25.68$ sec when the corresponding mode shift criteria (Table 4) were met.

Control about the roll axis changed from bank command (ϕ_{cmd}) to roll rate command (p_{cmd}) once the aircraft accelerated past 10 kt airspeed. The pilot, previously used to commanding bank angle directly using TCS, overcorrected at $t = 16$ sec while attempting to center the aircraft over the runway centerline with roll rate command, resulting in a brief $-22°$ bank angle excursion with $\pm 50°/s$ commanded roll rates. Once the aircraft entered TFM, control about the pitch axis changed from pitch attitude command (θ_{cmd}) to pitch rate command (q_{cmd}).

As this was the first transition attempt with TMS, the pilot moved the nacelles gradually and not aggressively at their maximum rate. Nevertheless, the acceleration from hover to forward flight using TMS took only 17.2 sec, compared to 21.8 sec using TCS (Fig. 9). A maximum performance acceleration from TMS can be accomplished in an even shorter time interval.

Decelerating Transition Using TMS

A decelerating transition performed using TMS is shown in Fig. 12. Onboard and external footage with telemetry is available on YouTube at https://tinyurl.com/TMS-decel.

After completing a base-to-final turn to align with the runway, the pilot initiated the deceleration by placing the LHI between detents D1 and D2, commanding a nacelle angle $\delta_{nac,\text{cmd}} > 7°$. TMS shifted from FFM into TFM once the airspeed fell below 40 kt, satisfying the applicable criteria (Table 4). This activated the lift propellers, whose thrust increased progressively thereafter. The pilot progressively moved the nacelles aft to an angle of 51°. TMS shifted from TFM to HFM once the nacelle angle exceeded 30° (Table 4).

The pilot then reversed the direction of flight by performing a teardrop-shaped turn (first to the right, then to the left) while initiating a descent. This coordinated turn was performed using roll rate command (p_{cmd}) with the nacelles set to 51°.

Once over the runway, the pilot switched from TMS to TCS. The control mode change occurred predictably without any transients. The pilot then engaged auto-flight functions CTL and LANDING to track towards and land on the runway centerline.

Aileron Rolls in TMS

To test maneuvering in TMS control mode beyond usual attitudes, two aileron rolls were executed in FFM with mode transitions disabled (LOCKED). These are shown in Fig. 13 and onboard footage of the maneuvers is available on YouTube at https://tinyurl.com/TMS-roll.

Starting from an airspeed of approximately 60 kt, the pilot pitched up to approximately 40° nose-up pitch attitude

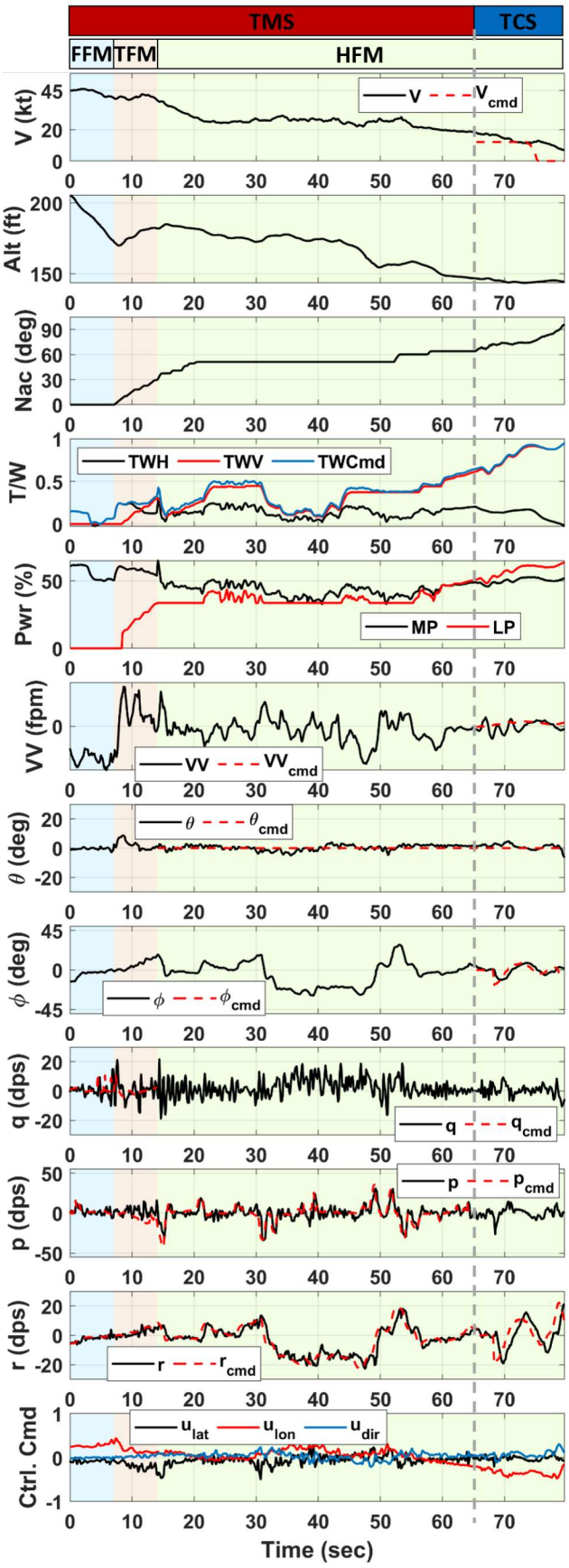

Figure 12. Decelerating transition using TMS

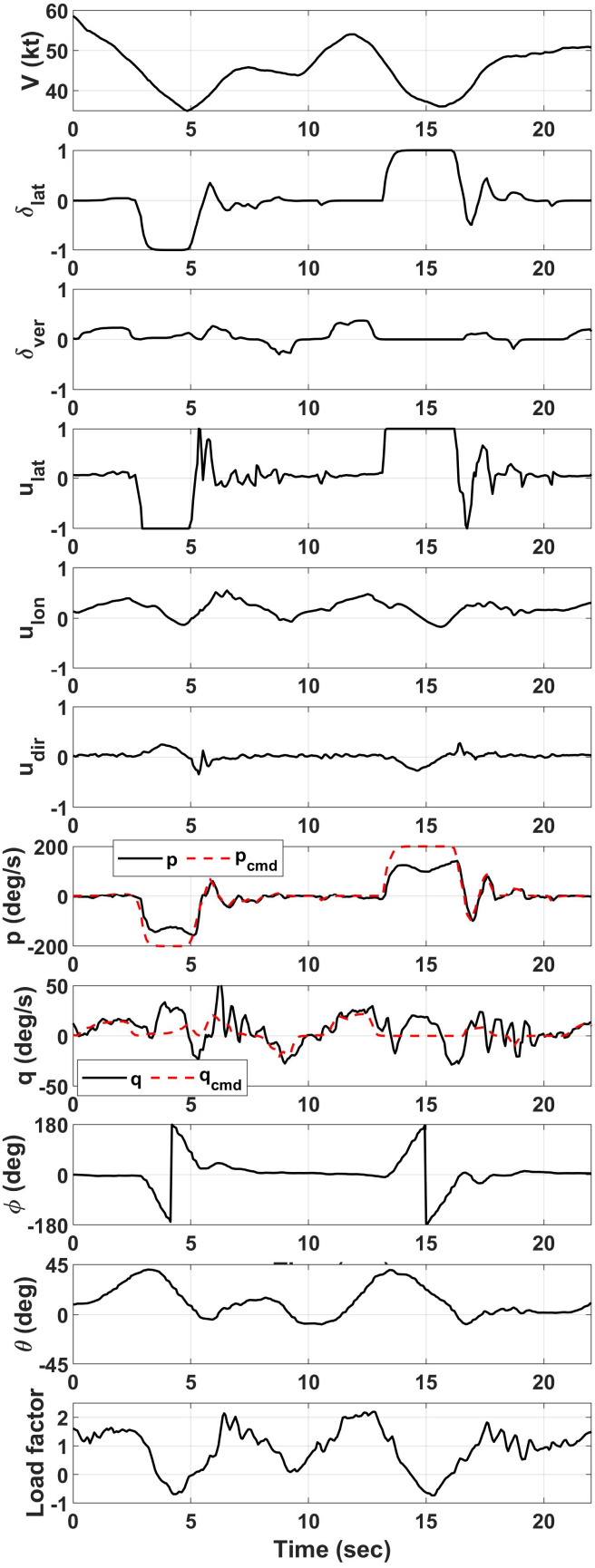

Figure 13. TMS aileron rolls (left and right)

and applied full-left RHI input ($\delta_{lat} = -1$), commanding a $-200°/s$ roll rate. The aircraft completed the aileron roll, but did not achieve the roll rate target. With full roll control effort $u_{lat} = -1$, corresponding to full anti-symmetric flaperon deflections, a peak roll rate of $-158°/s$ was achieved.

Upon completion of the first roll, the pilot dove for airspeed, pulled up to a 40° nose-up pitch attitude, and applied full-right RHI input ($\delta_{lat} = +1$), commanding a $+200°/s$ roll rate. With full roll control effort ($u_{lat} = +1$) through anti-symmetric flaperon deflections, the peak roll rate achieved was $+142°/s$, once again falling short of the command. However, the limiting factor here is the aircraft roll control authority, not the roll axis control law.

CTOL Operations

CTOL operations have been tested with TCS active. When CTOL operating mode is selected on the ground, the flight mode switches to FFM and subsequent mode transitions are disabled (LOCKED). For the VT-03-s Shadow configuration, this causes the nacelles to move to their forward flight position while the lift propulsors deactivate. The CTL function tracks the runway centerline on the ground using differential thrust to steer the aircraft. During the takeoff roll, takeoff rotation is induced through the $\theta_{\text{cmd},4}$ term of the TCS FFM pitch control law (Eq. 11). Several conventional takeoffs (both manually piloted and autonomous) have been successfully demonstrated during flight-testing.

For a conventional landing, the CTL and LANDING functions can be used together, the former tracking the runway centerline and the latter commanding a vertical velocity corresponding to a target flightpath angle. Alternatively, the final approach can also be flown using the NAV function, in which case two waypoints are used to define the final approach path. In both cases, once the aircraft reaches a programmed round-out height, the LANDING function reduces the descent rate with decreasing height above the ground, while the speed command is gradually decreased, inducing the landing flare. Presently, the round-out and flare characteristics are being adjusted.

CONCLUSIONS

This work demonstrated a novel Maneuver Control System (MCS) for the VT-03-s Shadow subscale aircraft comprising two distinct flight control modes, the Trajectory Control System (TCS) intended for Simplified Vehicle Operations (SVO), and the Tactical Maneuvering System (TMS) intended for more aggressive maneuvering flight. The two control modes perform distinct control actions over the speed envelope, comprising Hybrid Flight Mode (HFM), Transition Flight Mode (TFM), and Forward Flight Mode (FFM).

TCS computes the main and lift propulsor thrust, nacelle angle, and pitch attitude required to achieve upstream trajectory commands. TMS, on the other hand, allows the pilot more direct control over the above, with the resulting vehicle trajectory being a fallout. Each has its advantages and disadvantages, and neither is superior to the other. Both TCS and TMS are harmonized within the MCS with the rest of the flight control architecture, allowing transient-free in-flight switching between the two control modes, which is one of the salient features of the demonstrated flight control architecture.

The capabilities of both control modes have been demonstrated through flight-testing, which has included both vertical takeoff and landing (VTOL) and conventional takeoff and landing (CTOL) operations. Transitions between hover and forward flight were first demonstrated using TCS as part of an autonomous flight profile. This was followed by manually piloted transitions performed using TMS. In both cases, stable and predictable flight characteristics were obtained. As expected, the pilot workload was higher with TMS due to the absence of SVO-centric envelope-limiting and hold functions and prior pilot experience with TMS. Command tracking was acceptable with both control modes, though vertical velocity tracking in TFM and an airspeed overshoot upon reaching FFM with TCS active will be addressed in future flight-testing. The rate-based TMS control logic was also tested in FFM in unusual attitudes through basic aileron rolls where the commanded roll rate resulted in full deflection of the roll control effectors (flaperons).

Flight-testing performed to date has established VT-03-s Shadow as a versatile VTOL/CTOL configuration serving as a testbed for advanced flight control architectures. It also demonstrated that the MCS is an effective middle-loop controller, combining the SVO characteristics of TCS with the enhanced maneuvering capabilities of TMS, allowing either to be selected in-flight based on the requirements of the phase of flight.

Future flight-testing will include a formal system identification campaign to identify the on-axis transfer functions of the aircraft at different flight conditions, incorporate these into its MADCASP simulation model, and use them to enhance the feedforward characteristics of the explicit model-following inner-loop control system.

REFERENCES

1. General Aviation Manufacturers Association (GAMA). A Rational Construct for Simplified Vehicle Operations (SVO) - Whitepaper Version 1.0. online: https://shorturl.at/bjreh, 2019. [Online; accessed April 14, 2026].

2. A. Comer and I. Chakraborty. Flight control system architecture for urban air mobility simplified vehicle operations. In *AIAA SCITECH 2023 Forum*, National Harbor, MD, January 2023. AIAA-2023-0399.

3. A. Comer and I. Chakraborty. Total energy-based control architecture design and optimization for a lift-plus-cruise aircraft. *AIAA Journal of Guidance, Control, and Dynamics*, 47(7):1414–1436, 2024.

4. A. Comer, R. Bhandari, S.H. Putra, and I. Chakraborty. Design, control law development, and flight testing of a subscale lift-plus-cruise aircraf. In *AIAA SCITECH 2024 Forum*, Orlando, FL, January 2024. AIAA-2024-2644.

5. A. Comer, A. Mishra, and I. Chakraborty. Total energy flight control architecture optimization for a tilt-wing aircraft. In *AIAA AVIATION 2023 Forum*, San Diego, CA, June 2023. AIAA-2023-4510.

6. A. Comer and I. Chakraborty. Full envelope flight control system design and optimization for a tilt-wing aircraft. *Journal of the American Helicopter Society*, 69(3):1–18, 2024.

7. A. Comer and I. Chakraborty. Explicit model following trajectory control system for multiple vertical takeoff and landing configurations. In *34th ICAS Congress*, Florence, Italy, September 2024. ICAS-2024-1166.

8. A. Comer, I. Chakraborty, Y. Kovryzhenko, E. Taheri, R. Bhandari, B Kunwar, and S.H. Putra. Flight testing of explicit model-following trajectory control system for lift-plus-cruise and tilt-wing configurations. In *VFS 80 Forum*, Montreal, QC, Canada, May 2024. Vertical Flight Society.

9. A. Comer, I. Chakraborty, S.H. Putra, R. Bhandari, B. Kunwar, and B. Davis. Design, optimization, and flight testing of a trajectory control system for lift-plus-cruise vtol aircraft. In *AIAA AVIATION 2024 Forum*, Las Vegas, NV, September 2024. AIAA-2024-4563.

10. I. Chakraborty and A. Comer. Optimizing explicit model-following trajectory control laws for a vectored thrust configuration. In *VFS 80 Forum*, Montreal, QC, Canada, May 2024. Vertical Flight Society.

11. Imon Chakraborty, Bikash Kunwar, Stefanus H. Putra, Rajan Bhandari, and Henry C. McCormick. Flight-Testing of the VT-03-s Shadow Multi-Tilt-Rotor Configuration in VTOL and CTOL Operations. In *AIAA SCITECH 2026 Forum*. American Institute of Aeronautics and Astronautics. eprint: https://arc.aiaa.org/doi/pdf/10.2514/6.2026-2084.

12. Imon Chakraborty, Bikash Kunwar, and Peter Schmidt. A Maneuver Control System Enabling Simplified Vehicle Operations and Tactical Maneuvering for a Tilt-Wing Aircraft. In *https://doi.org/10.4050/F-0081-2025-406*. The Vertical Flight Society, May 2025.

13. Brian German, Ayush Jha, Jason Welstead, Siena Whiteside, and Nathaniel J. Blaesser. Design and Programmatic Overview of the Research Aircraft for eVTOL Enabling techNologies (RAVEN) Activity. In *AIAA AVIATION 2023 Forum*, San Diego, CA and Online, June 2023. American Institute of Aeronautics and Astronautics. https://arc.aiaa.org/doi/10.2514/6.2023-3924.

14. M. Tischler, T. Berger, C. Ivler, M. Mansur, K. Cheung, and J. Soong. *Practical Methods for Aircraft and Rotorcraft Flight Control Design - An Optimization-Based Approach*. American Institute of Aeronautics and Astronautics, 1st edition, 2017.

15. I. Chakraborty and A. Mishra. Sizing and analysis of a lift-plus-cruise aircraft with electrified propulsion. *AIAA Journal of Aircraft*, 60(3):747–765, 2022.

16. Bikash Kunwar, Aashutosh A Mishra, Rajan Bhandari, and Imon Chakraborty. Sizing and optimization of an urban air mobility aircraft using parametric aero-propulsive model. In *AIAA AVIATION 2023 Forum*, San Diego, CA, 2023. AIAA-2023-3662.

17. Bikash Kunwar, Aashutosh A Mishra, and Imon Chakraborty. Sizing and analysis of canard-wing aircraft with jet propulsion. In *AIAA AVIATION FORUM AND ASCEND 2024*, Las Vegas, NV, 2024. AIAA-2024-3752.

18. John Deyoung. Theoretical symmetric span loading due to flap deflection for wings of arbitrary plan form at subsonic speeds, January 1952. NTRS Author Affiliations: NTRS Report/Patent Number: NACA-TR-1071 NTRS Document ID: 19930092116 NTRS Research Center: Legacy CDMS (CDMS).

19. R.D. Finck. United States Air Force Stability and Control DATCOM (Data Compendium). Technical report, McDonnell Aircraft Co., St. Louis, MO, 1978.

20. Jinggen Zhao. *Dynamic Wake Distortion Model for Helicopter Maneuvering Flight*. PhD thesis, Georgia Institute of Technology, Atlanta, GA, USA, March 2005.